Mathematical models of gas hydrate accumulation

A. W. REMPEL[1] & B. A. BUFFETT[2]

[1]*Institute of Theoretical Geophysics, Department of Applied Mathematics and Theoretical Physics, University of Cambridge, Silver Street, Cambridge, UK*

[2]*Department of Earth and Ocean Sciences, University of British Columbia, 2219 Main Mall, Vancouver, Canada*

Abstract: Gas hydrate reservoirs are widespread on the world's continental margins and in the Arctic, but little is known about the way in which they form. We use conservation principles to derive a set of equations that describe hydrate formation in uniform porous media. Using scaling arguments, we identify the physical processes that are most important to hydrate accumulation in different environments. This knowledge is used to construct models that quantitatively predict the development of hydrate layers under a variety of circumstances. These models compare favourably with recent field observations of hydrates in marine sediments.

How much gas is contained in a given hydrate reservoir and how is it distributed? These questions are of paramount importance in determining the impact of these deposits on margin stability, the global climate, future energy concerns and the methane budget. To address these issues properly, we must also know why the gas is distributed as it is and how long it takes to accumulate. Extensive exploration using bore hole (e.g. Kvenvolden & Bernard 1983; Brooks *et al.* 1985; Kastner *et al.* 1995; Dickens *et al.* 1997) and seismic techniques (e.g. Hyndman & Spence 1992; Minshull *et al.* 1994; Yuan *et al.* 1996) has provided insight into the present-day characteristics of hydrate deposits at numerous locations around the world. Researchers have extrapolated these observations to estimate the total volume of carbon contained in these reserves globally (Kvenvolden 1993; Holbrook *et al.* 1996). These ongoing studies will continue to improve our understanding of the current state of the hydrate deposits found on our continental margins and in the Arctic. Unfortunately, however, these methods provide little information regarding the reasons for the observed spatial distribution of hydrate at a given reservoir and the duration over which the hydrate has accumulated.

The accumulation rate and spatial distribution of hydrate are determined by the physical conditions at each location. We can predict the amount of hydrate we expect to encounter in a particular reservoir by modelling the ways in which the various physical processes interact. Field observations and laboratory simulations can be used to help refine these models and improve our understanding of the potential of these deposits. Alternatively, with accurate data on the distribution of hydrates within a reservoir, we can use models of hydrate accumulation to address the question of how the hydrate saturation acquired its present profile. Models of hydrate dissociation have been developed previously (Selim & Sloan 1989; Tsypkin 1991, 1992*a*,*b*), but little quantitative work on modelling hydrate formation under geological conditions has been reported in the literature.

In the current paper we present models of hydrate accumulation in different physical environments. We begin by outlining the stability requirements necessary for hydrates to be in equilibrium with their surroundings. This leads to a discussion of the governing equations that describe how hydrate deposits form in uniform porous media. Next, we use scaling arguments to delineate physical effects that are most important in various circumstances. Finally, we give a few illustrative examples of the predictions of some models of hydrate accumulation in uniform porous media and discuss their implications.

Stability requirements

The three-phase equilibrium conditions necessary for the stable coexistence of hydrate, water, and free gas are determined by the hydrate former and the pore-water chemistry (e.g. Englezos & Bishnoi 1988; Sloan 1990; Dickens & Quinby-Hunt 1997). On continental margins, the high pressures and relatively low temperatures in the shallow sediments provide a stable environment for hydrates when there is sufficient gas (see Fig. 1). Knowledge of the hydrostatic pressure, the geothermal gradient and the appropriate three-phase equilibrium curve is sufficient

REMPEL, A. W. & BUFFETT, B. A. 1998. Mathematical models of gas hydrate accumulation. *In:* HENRIET, J.-P. & MIENERT, J. (eds) *Gas Hydrates: Relevance to World Margin Stability and Climate Change*. Geological Society, London, Special Publications, **137**, 63–74.

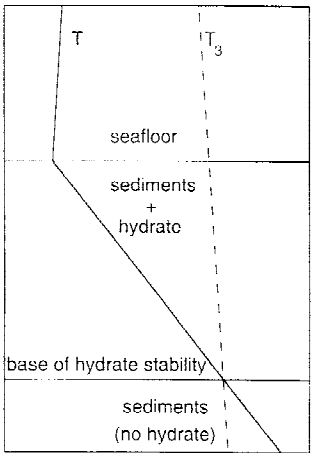

Fig. 1. A schematic representation of the thermal conditions near the sea floor. The dashed line represents the temperature T_3 for three-phase equilibrium between hydrate, pore fluid and free gas at the hydrostatic pressure. Hydrate is stable in the upper region of the sediment column where the temperature T falls below T_3; beneath this level, hydrates are no longer stable.

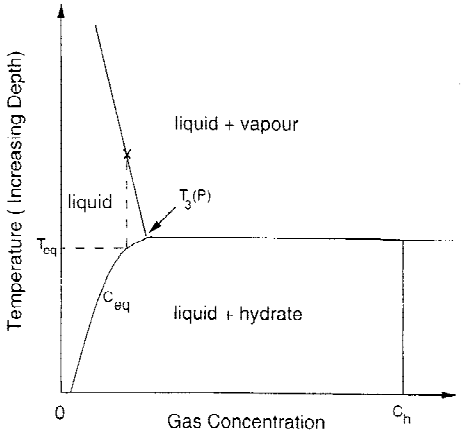

Fig. 2. A schematic representation of a portion of the phase diagram of a gas–water system at constant pressure. In the case of a closed system which is cooled from the point marked X, hydrate does not begin to form until some temperature T_{eq}, which is less than the three-phase equilibrium temperature $T_3(P)$. As the system is cooled below T_{eq} hydrate continues to form with gas mass fraction c_h as the gas concentration in solution is depleted along the curve marked c_{eq}.

to estimate where and to what depth the stability zone extends. (In general, sediment properties may alter the three-phase equilibrium through the (Gibbs–Thompson) effects of curvature for example (Clennell *et al.* 1995); these complications act to adjust the pressure–temperature conditions for three-phase equilibrium, and in principle they may be accounted for in the choice of the appropriate three-phase equilibrium curve.) The stability boundary is often marked by a bottom simulating reflector (BSR) in seismic experiments, which is caused by a jump in acoustic impedance as hydrate-bearing sediments give way to fluid-saturated sediments which can contain free gas (e.g. Bangs *et al.* 1993; MacKay *et al.* 1994; Singh & Minshull 1994; Yuan *et al.* 1996). When the sediment permeability is too low to permit the transport of free gas away from the three-phase equilibrium boundary, a plane of weakness can develop at the BSR and lead to sediment failure.

While the three-phase equilibrium conditions determining the base of the hydrate stability field have received much attention and are fairly well known (e.g. Englezos & Bishnoi 1988; Sloan 1990; Dickens & Quinby-Hunt 1997), the two-phase equilibrium conditions which prevail above the base of the stability zone have been the subject of comparatively little research. If sufficient gas is available, we expect the pore space within the stability region to be occupied by a combination of solid hydrate and aqueous solution (Handa 1990). (In extremely gas-rich environments, it is possible to envision a two-phase equilibrium between hydrate and a mixture of free gas and water vapour, but this is not expected to be a common arrangement in the sea floor.) In a two-phase region with hydrate and aqueous solution, the equilibrium gas concentration dissolved in the water is a function of the *in situ* temperature and pressure. Experimental evidence and theoretical predictions show that the solubility of gas in water decreases when the system is brought further into the hydrate stability field by either increasing the pressure or reducing the temperature (Handa 1990; Yamane & Aya 1995; Zatsepina & Buffett 1997). (The presence of salts and multiple gas components will affect the value of the equilibrium gas concentration, but the basic form of the temperature and pressure dependence will be similar.) As shown in Fig. 2, this is the opposite of what occurs outside the hydrate stability field, where gas solubility is enhanced by increased pressure or decreased temperature (Fogg & Gerrard 1991). Because temperature largely controls the solubility behaviour under geological conditions, hydrate can crystallize from a gas-saturated aqueous solution without the presence of any free gas. Free gas

would normally only be found beneath the gas hydrate zone. (The possibility that the effects of crystal growth kinetics may allow free gas to persist well into the hydrate stability zone will be discussed later.)

Governing equations

The interactions of several competing physical processes determine the rate of accumulation and spatial distribution of hydrate in a developing reservoir. As gas is removed from the interstitial fluid and incorporated into the hydrate structure, there is an associated latent heat release. The local hydrate accumulation rate is dependent on how quickly additional gas can be supplied and latent heat can be removed by advective and diffusive processes. By modelling the sediment–hydrate–liquid system as a continuum, we can use conservation principles to derive equations that describe these interactions. We restrict our attention to single-component hydrates in sediments which initially contain pure water, although our arguments may be easily modified to consider multi-component hydrates and the presence of salts. (The dynamics of heat and mass transport which control the hydrate accumulation process also govern the formation of mushy layers during the solidification of a binary melt. This related class of problems contains many fundamental similarities to the hydrate accumulation problem (e.g. Huppert & Worster 1985; Worster 1992).)

We consider the hydrate reservoir to consist of a uniform porous medium in which the void space ϕ is partitioned into hydrate, with pore-volume fraction h, and an aqueous solution with pore-volume fraction $1-h$ and gas concentration c (see Appendix 1 for a list of symbols and their definitions). The latent heat of formation L and the mass fraction of gas contained in the hydrate c_h are treated as constants; as are the densities ρ and specific heats C of each of the components (subscripts: s = sediment, h = hydrate, f = fluid). The bulk thermal conductivity $K(h)$, the bulk heat capacity $\bar{C}(h)$, and the combined diffusion–dispersion coefficient $D(h)$ all depend on the amount of hydrate present, h.

Heat and gas are transported both through the fluid by advection, and by diffusion and dispersion down the temperature and gas concentration gradients. Latent heat release provides a source of heat as hydrate is produced, and the gas which is incorporated into the hydrate structure reduces the aqueous solution's gas content. The conservation of energy and gas lead to the primary governing equations which describe how these processes change the temperature T and the mass fraction of gas in the fluid c (Rempel 1994; Rempel & Buffett 1997); (Appendix 2 contains a brief derivation)

$$\bar{C}(h)\frac{\partial T}{\partial t}+\mathbf{u}\cdot\nabla t=\nabla\cdot(\kappa(h)\nabla T)+\frac{\rho_h\phi L}{\rho_f C_f}\frac{\partial h}{\partial t}$$

and

$$(1-h)\frac{\partial c}{\partial t}+\frac{1}{\phi}\mathbf{u}\cdot\nabla c=\nabla\cdot[(1-h)D(h)\nabla c]-\frac{\rho_h}{\rho_f}(c_h-c)\frac{\partial h}{\partial t} \qquad (1)$$

where the effective thermal diffusivity

$$\kappa(h)\equiv\frac{K(h)}{\rho_f C_f}$$

is defined as the ratio of the bulk thermal conductivity to the heat capacity of the fluid, and the bulk heat capacity is

$$\bar{C}(h)\equiv\frac{\rho_f C_f\phi(1-h)+\rho_h C_h\phi h+\rho_s C_s(1-\phi)}{\rho_f C_f}.$$

The fluid velocity $\mathbf{u}$ is altered by the reduction in effective permeability $k(h)$ which must accompany the reduction in effective porosity when hydrate occupies a portion of the pore space. In addition, the density difference between hydrate and the pore fluid will cause a divergence in flow as hydrate forms. These effects are described by Darcy's law and the continuity condition

$$\mathbf{u}=\frac{k(h)}{\eta}\nabla P'$$

and

$$\nabla\cdot\mathbf{u}=\frac{\phi(\rho_f-\rho_h)}{\rho_f}\frac{\partial h}{\partial t} \qquad (2)$$

where $\nabla P'$ is the non-hydrostatic component of the pressure gradient, and η is the dynamic viscosity of the pore fluid.

Within the hydrate reservoir, the equilibrium condition gives a relationship between the fluid's gas concentration and the temperature. In principle the equilibrium concentration depends on both pressure and temperature, but in geological applications the temperature dependence is expected to be the controlling factor. The temperature dependence of c_{eq} may be expressed in the convenient form

$$c_{eq}(T)=c_{eq}(T_3)\exp[\alpha(T-T_3)] \qquad (3)$$

where T_3 is the temperature for three-phase equilibrium and $c_{eq}(T_3)$ is the corresponding solubility. The two-phase equilibrium calculations of Zatsepina & Buffett (1997) show that $\alpha^{-1}\approx 10°C$ for the methane hydrate–water

system in the range of temperature–pressure conditions that represent marine sediments.

Crystal growth kinetics can lead to departures from the equilibrium state. Kinetic effects have been the subject of numerous laboratory studies (e.g. Englezos *et al.* 1987; Sloan 1990), but many details remain poorly constrained. Given the uncertainties involved, we choose to model non-equilibrium effects by adopting a simple linear equation in which the rate of gas consumption is proportional to the concentration in excess of the equilibrium value

$$\frac{dc}{dt} = -\Re(c - c_{eq}) \tag{4}$$

where $\Re$ is the reaction-rate constant.

Scaling arguments

To assess the relative importance of the different terms in equation (1) we compare coefficients in the corresponding dimensionless equations. We introduce the dimensionless temperature $\tilde{T} = (T - T_0)/\Delta T$ and gas concentration $\tilde{c} = (c - c_0)/\Delta c$, where ΔT and Δc are typical variations over the region of interest, and T_0 and c_0 are convenient reference values. Hydrate deposits are normally located in regions where the temperature and the equilibrium dissolved gas concentration change most rapidly in the vertical dimension. The fluid flow is also often oriented in a predominantly vertical direction. For simplicity then, it is reasonable to restrict our attention to one-dimensional problems and write the dimensionless form of equation (1) as

$$\bar{C}(h)\frac{\partial \tilde{T}}{\partial \tilde{t}} + Pe\frac{\partial \tilde{T}}{\partial \tilde{z}} = \frac{\partial}{\partial \tilde{z}}\left(\frac{\kappa(h)}{\kappa(0)}\frac{\partial \tilde{T}}{\partial \tilde{z}}\right) + S\frac{\partial h}{\partial \tilde{t}}$$

and

$$(1-h)\frac{\partial \tilde{c}}{\partial \tilde{t}} + \frac{1}{\phi}Pe\frac{\partial \tilde{c}}{\partial \tilde{z}} \varepsilon \frac{\partial}{\partial \tilde{z}}\left((1-h)\frac{D(h)}{D(0)}\frac{\partial \tilde{c}}{\partial \tilde{z}}\right) - \frac{\rho_h}{\rho_f}(\tilde{c}_h - \tilde{c})\frac{\partial h}{\partial \tilde{t}} \tag{5}$$

where the dimensionless position is $\tilde{z} = z/l$, with l chosen as a typical length scale, and time is made dimensionless using the thermal diffusion time scale $\tilde{t} = t\kappa(0)/l^2$. Provided we choose the length scale l and the temperature and gas concentration scales, ΔT and Δc, appropriately, the derivatives in equation (5) will be roughly the same order of magnitude and the size of their dimensionless coefficients will indicate the relative importance of the various terms.

The new parameters introduced in equation (5) are the Peclet number, Pe the Stefan number, S, the Lewis number, ε, and the dimensionless hydrate gas concentration, $\tilde{c}_h$. The Peclet number,

$$Pe = \frac{ul}{\kappa(0)}$$

measures the speed with which heat can be transported through the fluid by advection, at fluid velocity u, relative to the speed with which it is conducted through the sediment–fluid mixture ($\kappa(0)$ is the thermal diffusivity in the absence of hydrate, i.e. $h = 0$). The Stefan number,

$$S = \frac{\rho_h \phi L}{\rho_f C_f \Delta T}$$

indicates the relative importance of the latent heat which is liberated as hydrate is produced compared to the heat required to change the temperature. The Lewis number,

$$\varepsilon \equiv \frac{D(0)}{\kappa(0)}$$

is defined as the ratio of the combined diffusion and dispersion coefficient for dissolved gas transport (with $h = 0$) to the thermal diffusion coefficient $\kappa(0)$. The dimensionless hydrate gas concentration,

$$\tilde{c}_h \equiv \frac{c_h - c_0}{\Delta c}$$

is the ratio of the difference between the mass fraction of gas in the hydrate c_h and the reference gas concentration in the fluid c_0, to typical variations in fluid gas content Δc. The high gas storage capacity of hydrates ensures that c_h is always much larger than the amount of gas which can be dissolved in the fluid, so $c_h \gg c_0$ and $\tilde{c}_h \approx c_h/\Delta c$.

The thermal conductivities of hydrate and water differ by about 10–20% depending on the hydrate former (Sloan 1990). As this difference is relatively small, and heat is also transported through the sediment and the pore fluid, we can expect the ratio of the bulk thermal diffusivity of hydrate-bearing sediments to the bulk thermal diffusivity of hydrate-free sediments $\kappa(h)/\kappa(0)$ to be of the order of 1. Thus, by comparing the coefficients in equation (5) we see that thermal diffusion dominates the heat transport if the Peclet number is much less than 1, and advective transport dominates if Pe is much greater than 1. On the Cascadia margin, where extensive hydrate deposits are found, the background fluid velocity is of the order of several millimetres per year (Hyndman *et al.* 1993). A typical vertical dimension for a hydrate deposit is roughly 10^2 m, and typical thermal diffusivities are on the order of $10^{-7}\,m^2\,s^{-1}$ (Davis *et al.* 1990). In

this case the Peclet number is much less than 1 ($Pe \approx (10^{-11}\,\mathrm{m\,s^{-1}})(10^{2}\,\mathrm{m})/(10^{-7}\,\mathrm{m^2\,s^{-1}}) \approx 10^{-2}$) and therefore advection of heat can be neglected when modelling the large-scale hydrate accumulation. In the same reservoir, however, fluid velocities in localized cracks and faults might be several orders of magnitude higher than the background field. In these local environments, where the Peclet number is large, it is essential to retain the advective term in models of hydrate accumulation.

In the equation for $\tilde{c}$ we compare the Peclet number and the Lewis number to determine the principal mechanism for transporting gas. The compositional diffusivities of dissolved hydrocarbons in sedimentary rocks vary over several orders of magnitude (Kroos & Leythaeuser 1988). In general we expect thermal diffusion to be more efficient than chemical diffusion so the Lewis number is usually very much less than 1. With the large uncertainty involved in estimating $D(0)$, however, it is difficult to ascertain whether advection or diffusion dominates gas transport. Flow in cracks and faults can enhance advective transport, but it also seems reasonable to expect diffusive transport to be important in reservoirs where the large scale fluid velocity is only a few millimetres or less per year.

In laboratory hydrate formation experiments, non-equilibrium effects have been shown to control the rate of gas consumption when vigorous stirring is used to enhance the transport of gas and heat. The methane hydrate formation experiments of Uchida & Narita (1996) give reasonable fits to the empirical first-order equation (4) when $\Re$ is of the order of $10^{-3}\,\mathrm{s^{-1}}$. When the time scale $\Re^{-1}$ for non-equilibrium effects is short compared to the shortest time scale for the transport of heat and gas, we can assume that the gas concentration in the two-phase region is close to the equilibrium value given by equation (3). In many situations the shortest time scale for transport is the thermal diffusion time $l^2/\kappa(0)$ which can be several orders of magnitude larger than $\Re^{-1}$. In these cases we infer that the equilibrium assumption is valid. In cracks and fractures, however, the advective time scale l/u might be comparable to $\Re^{-1}$, and the non-equilibrium effects described by equation (4) become more important. Non-equilibrium effects could also play an important role in laboratory simulations, where the fluid velocity is negligible but the length scale is short.

Hydrate accumulation models

Idealized physical models are useful for illustrating some of the important features of solutions to the governing equations. For example, a simple model can be obtained for the case of a uniform porous half-space cooled on its boundary to a temperature T_0 less than the equilibrium temperature T_{eq} (see Fig. 3). In this case, the fluid velocity, and hence the Peclet number, is initially zero. A divergence of flow is produced by the volume change due to hydrate formation, according to equation (2), but the associated velocities are small so the Peclet number remains close to zero and advective transport of heat and gas may be neglected. When the Lewis number is also small the diffusive gas transport is much slower than the diffusive heat transport. The temperature drops quickly relative to the speed of gas transport, so the gas cannot move appreciably before the temperature drops below the two-phase equilibrium temperature given by equation (3) and hydrate begins to form. Ther-

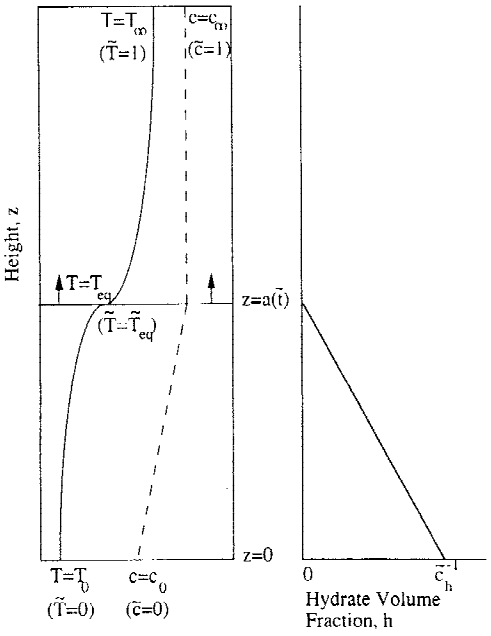

Fig. 3. A schematic representation of the temperature, fluid gas concentration and hydrate volume fraction profiles for a uniform porous half-space cooled on its boundary. Initially, the temperature is constant at T_∞ and the gas concentration is constant at c_∞. The base at $z = 0$ is then cooled to a temperature T_0 (where the corresponding equilibrium gas concentration is c_0). A hydrate layer develops with an advancing interface at $z = a(t)$ along which the temperature is equal to the equilibrium value T_{eq}. The hydrate volume fraction in the layer is a function of both position and time, and decreases from a high of $\tilde{c}_h^{-1}$ at the base, to zero at the moving interface.

mal diffusion determines the position of the moving phase change interface separating the growing two-phase hydrate stability region from the warmer gas-rich aqueous solution. Given a constant initial temperature T_∞ and gas concentration c_∞, the problem reduces to become a member of the well-known class of solidification problems known as Stefan problems (e.g. Turcotte & Schubert 1982). The equations can be solved analytically to give expressions for the hydrate volume fraction and the growth rate of the layer (Rempel & Buffett 1997).

This model for hydrate formation in a porous half-space gives the hydrate volume fraction as approximately

$$h \approx \frac{1 - \tilde{c}}{\tilde{c}_h} \tag{6}$$

where $\tilde{c}$ is the dimensionless form of the two-phase equilibrium concentration and the values of c_0 and Δc used to define $\tilde{c}_h$ are the equilibrium gas concentration at the boundary and the difference between c_0 and the initial gas concentration c_∞. In practice, the large gas storage capacity of hydrates ensures that the dimensionless hydrate gas concentration $\tilde{c}_h$ is always much larger than the fluid gas concentration $\tilde{c}$, so the maximum value of h tends to be less than 1%. The hydrate distribution described by equation (6) decreases from a high of $\tilde{c}_h^{-1}$ at the chilled boundary to zero at the moving interface $a(\tilde{t})$ (see Fig. 3).

The position of the phase change interface is of the form $a(\tilde{t}) = 2\lambda\sqrt{\tilde{t}}$, where the constant λ is found by imposing energy conservation on the interface. An interesting feature of this problem is that the hydrate volume fraction at the interface goes to zero so there is no discontinuity in h at $a(\tilde{t})$; energy conservation implies that the temperature gradient must therefore be continuous across the interface. The most important parameters determining the value of λ, and hence the speed of the moving interface, are the Stefan number S, defined with $\Delta T = T_\infty - T_0$, and the dimensionless equilibrium temperature $\tilde{T}_{eq} = (T_{eq} - T_0)/(T_\infty - T_0)$. The Stefan number measures the relative importance of the latent heat and the heat required to change the temperature. When S is high, the growth of the interface is slowed by the large heat release associated with the phase transition (see Fig. 4a). As S tends to zero, the latent heat release becomes negligible, and the only constraint on the growth rate of the layer is the time required to cool the sediments below the equilibrium temperature T_{eq}. When the initial temperature T_∞ is much warmer than T_{eq}, the dimensionless equilibrium temperature $\tilde{T}_{eq}$ is small; more heat must be extracted to cool the system, and the layer growth is slow (see Fig. 4b). When $\tilde{T}_{eq}$ is close to 1, the initial temperature is near the equilibrium temperature and the phase change interface moves rapidly.

In naturally occurring hydrate deposits, the manner in which the gas gets incorporated into the hydrate structure is a matter of some dispute. One theory holds that *in situ* biogenic gas production from buried organic material is the main gas source (Kvenvolden & Barnard 1983; Brooks *et al.* 1985). Others argue that there is insufficient organic material available to account for the large volumes of hydrate present, so there must be significant gas transport into the stability region from below (Hyndman & Davis 1992). Numerical solutions to the governing equations

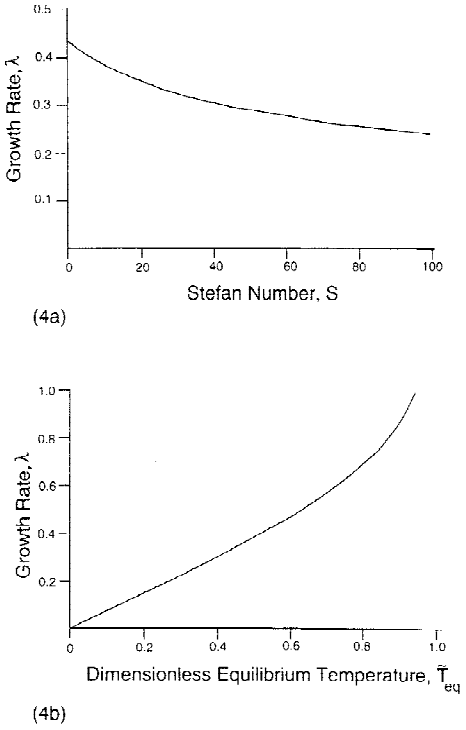

Fig. 4 (**a**) A plot of the growth-rate parameter λ as a function of the Stefan number $S \equiv \rho_h \phi L/(\rho_f C_f (T_\infty - T_0))$. At higher values of S, the growth rate is reduced by the need to remove more latent heat. (**b**) The dependence of λ on the dimensionless equilibrium temperature $\tilde{T}_{eq} \equiv (T_{eq} - T_0)/(T_\infty - T_0)$. When the equilibrium temperature T_{eq} equals the initial temperature T_∞, $\tilde{T}_{eq} = 1$ and layer growth is limited only by the need to remove latent heat.

can be used to explore the implications of these two models (Rempel & Buffett 1997).

For the gas flux model, we assume that the temperature profile is initially conductive and there is no gas in the hydrate zone. Beneath the level of the hydrate stability zone, the gas concentration is fixed at a constant value, and this gas is transported upwards by the combined effects of advection and diffusion. For typical parameter values (see Table 1) the temperature perturbations caused by hydrate production are insignificant, and the Peclet number is sufficiently small so that the temperature profile remains linear. After several thermal diffusion time cycles the gas concentration reaches a steady, equilibrium profile. When the Lewis number is small compared to the Peclet number the gas transport is dominated by advection and the hydrate accumulation rate is given by

$$\frac{\partial h}{\partial t} = -\frac{\rho_f \mathbf{u}\cdot\nabla c_{eq}}{\rho_h \phi (c_h - c_{eq})}. \qquad (7)$$

Using the relationship from equation (3) between c_{eq} and temperature, we infer from equation (7) that the rate of hydrate accumulation decreases exponentially upwards into the stability zone. This prediction yields a hydrate saturation profile that is highest near the BSR, consistent with some estimates based on field observations (see Fig. 5) (e.g. Brown *et al.* 1996; Yuan *et al.* 1996). Using parameter values representative of conditions in marine sediments (see Table 1), we get an additive increase in hydrate volume of order 1% of the pore space in 10^5 years near the base of the hydrate stability field.

For the *in situ* gas production model we initially assume that the gas production rate is uniform throughout the entire sediment column. When the temperature profile is conductive, as in marine sediments, the gas solubility behaviour suggests that hydrate should form most readily where the system is furthest into the hydrate stability field at the top of the sediment column. This would lead to a hydrate saturation profile with a hydrate volume fraction that decreases with depth. If we allow the temperature conditions in the sediments to evolve due to the effects of continuing sedimentation, however, we get a much different result. The temperature at the base of the stability field increases and the position of the BSR migrates upwards as hydrate dissociates to liberate free gas (see Fig. 6). This gas rises back into the stability region by advection and compositional diffusion, and the new hydrate it forms is concentrated near the BSR. The overall hydrate saturation profile that

Table 1. *Parameter values*

Property	Nominal value	Units
ρ_f	1000	kg m^{-3}
ρ_h	930	kg m^{-3}
ρ_s	2650	kg m^{-3}
C_f	4200	J kg^{-1} K^{-1}
C_h	2080	J kg^{-1} K^{-1}
C_s	2200	J kg^{-1} K^{-1}
ϕ	0.5	–
L	430	kJ kg^{-1}
$\kappa(0)$	10^{-7}	m s^{-2}
$D(0)$	10^{-9}	m s^{-2}
$\mathbf{u}$	10^{-11}	m s^{-1}
c_h	0.13*	–
c_0	10^{-3}†	–
α	0.1	K^{-1}
$\Re$	10^{-3}	s^{-1}
G	0.04	K m^{-1}

*Assumes $CH_4 \cdot 6H_2O$; †solubility of methane at 6.06 MPa and 298 K (Fogg & Gerrard 1991). Other sources are Lide (1990), Sloan (1990), Hyndman & Davis (1992), and Uchida and Narita (1996).

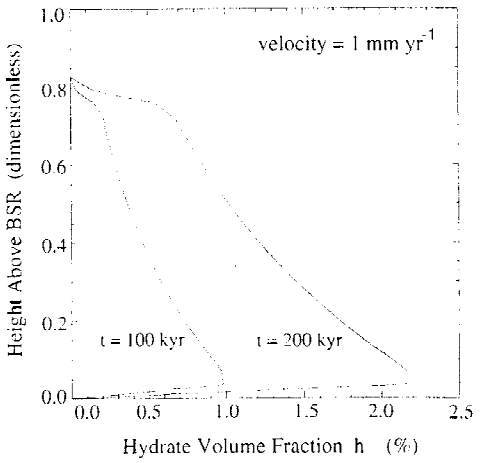

Fig. 5. The hydrate saturation profile for the gas flux model with a fluid velocity of 1 mm year^{-1}. The hydrate volume fraction decreases exponentially with height above the BSR. The ocean maintains the gas concentration at the sea water value at the sea floor (dimensionless height 1.0). This results in large gas concentration gradients near the sea floor, and compositional diffusion causes a sudden drop in hydrate volume fraction near dimensionless height 0.8. If the fluid velocity were higher, this drop in hydrate volume fraction would occur closer to dimensionless height 1.0.

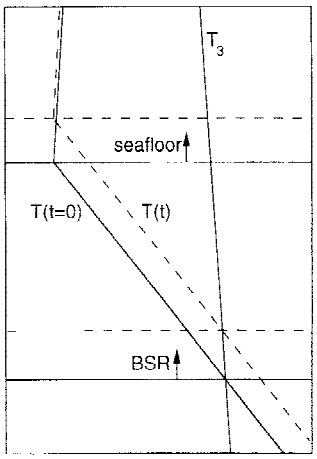

Fig. 6. A schematic diagram showing the effects of ongoing sedimentation on the temperature profile near the sea floor and on the position of the BSR. As time progresses and the sea-floor position migrates upwards, the temperature in the sediments changes from the solid line marked $T(t = 0)$ to the dashed line marked $T(t)$. The intersection of the geotherm and the three-phase equilibrium temperature T_3 migrates upwards, and hence the base of the stability region moves upwards as well.

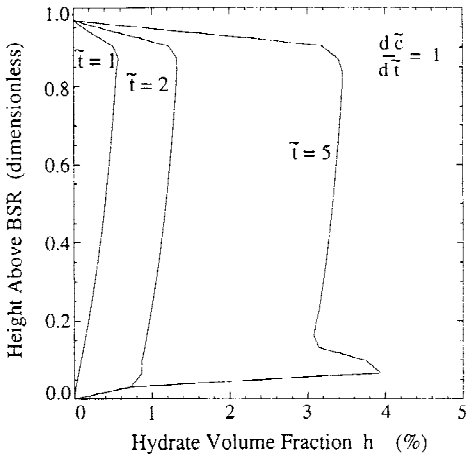

Fig. 7. The hydrate saturation level h as a function of dimensionless height above the initial BSR position for the *in situ* biogenic production model with the additional effects of sediment accumulation. The uniform dimensionless rate of biogenic gas production $d\tilde{c}/d\tilde{t}$ is 1. The sedimentation velocity is 0.01 so the new position of the BSR when $\tilde{t} = 5$ is 0.05. In this example the fluid velocity is zero so gas liberated from dissociated hydrate is transported back into the stability zone by compositional diffusion alone.

emerges from this scenario could contain two regions with an elevated hydrate volume fraction, similar to recent observations on the Blake ridge (Dickens *et al.* 1997). In Fig. 7, the upper region near the sea floor at dimensionless height 1.0 has an elevated hydrate volume fraction because of the decreased equilibrium gas concentration at lower temperatures. The peak in hydrate volume fraction near the BSR is caused by gas transported back into the stability region from hydrate that has dissociated because of the evolving thermal conditions. The time scale for this recycling of gas at the base of the stability zone depends on the rate of sedimentation and the rate of gas transport back into the stability zone, while the time scale for the total accumulation depends on the rate of biogenic gas production.

Discussion of model results

The observed vertical profiles of gas hydrate saturation in submarine deposits vary considerably from site to site. In addition, different methods of estimating hydrate saturation at the same location have yielded quite different results. For example, on the Cascadia margin, ODP Site 889, Yuan *et al.* (1996) found that velocity data from vertical seismic profiles and multi-channel seismic profiles suggest hydrate saturation levels of about 20% of the pore space immediately above the BSR, whereas chlorinity data indicate a pore saturation approaching 40% near the BSR. However, both data sets display the same general trend of increasing hydrate saturation levels with depth below the sea floor until a maximum is reached in the vicinity of the BSR. This is consistent with the predictions of the fluid-flux model of hydrate accumulation presented here (see Fig. 5). The fluid flux model suggests that hydrate saturation levels of order 10% of the pore space would require on the order of 10^6 years to accumulate.

Dickens *et al.* (1997) made direct measurements of methane content in recovered pressure core barrels at sites 995 and 997 of ODP Leg 164 on the Blake Outer ridge. They determined that the *in situ* methane concentration exceeds the two-phase hydrate liquid equilibrium concentration in a region from 190 to 450 m below the sea floor (mbsf). The data indicate two peaks in hydrate saturation; the first at approximately 200 mbsf, and the second, more prominent peak immediately above the BSR at 450 mbsf. These data are qualitatively similar to the predictions of the *in situ* gas production model with the effects of sedimentation (see

Fig. 7). Dickens *et al.* (1997) report that the sediments from 0 to 190 mbsf and from 240 to 380 mbsf appear not to contain enough methane to support significant amounts of hydrate. These observations could also be explained by the *in situ* production model if we allow the rate of biogenic gas production to vary with depth. For example, near the sea floor bacterial gas production is not expected to occur above the base of the sulphate reduction zone (Claypool & Kaplan 1974). In addition, variations in the amount of organic material available at different depths could result in different rates of biogenic gas production. Over certain depth ranges this could lead to insufficient biogenic production of methane to enable the local gas concentration to exceed the two-phase equilibrium value.

Caution must be exercised when comparing the model results to field observations. For example, while the upper peak in hydrate saturation at ODP Leg 164 can be explained by the *in situ* gas production model, it could also have resulted from enhanced gas migration accompanying hydrate dissociation during past climate change. Alternatively, if sediment failure were to occur immediately above a BSR it would change the position of the sea floor and the thermal conditions in the sediment. The free gas previously beneath the initial location of the BSR could be converted to hydrate and lead to a region of enhanced hydrate saturation well above the subsequent depth of the base of the hydrate stability zone. The models presented here do not account for sea-level changes or sediment failure, which could both strongly influence the hydrate saturation profile. In principle, these effects would not alter the form of the governing equations (1), and the current models could be modified to consider such events. With the limited amount of data currently available, however, it could be difficult to determine which of the various model scenarios best explains the observed hydrate distribution.

Hydrate saturation profiles determined using bore hole techniques can be heavily influenced by anomalous zones containing segregated hydrate. Segregated hydrate can result from enhanced fluid transport in confined regions or from the influence of the sediment properties on hydrate formation (Clennell *et al.* 1995). Fractures can act as preferred fluid migration pathways where the rapid flow increases the gas flux. The hydrate accumulation models presented in this study have all been applied to uniform porous media. The actual geological settings where hydrate deposits are found can be much more complex. However, the general form of the equations in equation (1) should not be altered by features such as fractures. Hydrate accumulation is still controlled by balances between advection and diffusion of gas and heat, and the latent heat release and gas consumption associated with the phase change. When modelling hydrate accumulation in non-isotropic and inhomogeneous media, solutions to the governing equations, must be fully three dimensional. These complications are beyond the scope of the current paper, but the basic physical processes are described by equation (1).

Conclusions

We have presented a set of governing equations which describes the accumulation of hydrate in porous media. We use scaling arguments to show that simplifications to the governing equations are justified in a number of physical settings. This allows us to produce simple models that describe how hydrate deposits form.

We first examined the case of an isothermal porous half-space cooled on its boundary. We found that the growth rate of the stability zone is controlled by thermal diffusion, while the hydrate saturation profile is determined by the gas available in excess of the equilibrium concentration. Next we looked at the results of two numerical models of hydrate accumulation in a region with a conductive thermal profile similar to that found in marine sediments. In the fluid flux model, we considered the development of a hydrate layer as gas is advected and diffused into the layer from below. For the case where advection dominates the gas transport, we obtained a simple expression for the change in hydrate volume fraction with time after a steady-state equilibrium gas concentration profile has developed. The predicted rate of increase in hydrate saturation level is greatest at the base of the stability field, which is consistent with some indirect observations of hydrate deposits. For the *in situ* biogenic production model coupled with ongoing sedimentation, we obtained a similar saturation profile to that for the fluid flux model. One of the principal differences between the two models is the suggestion of two possible regions with elevated hydrate saturation in the biogenic model. The upper maximum is caused by the reduced gas solubility at lower temperatures in the hydrate zone, while the lower maximum is caused by the redistribution of gas from dissociated hydrate as the geotherm migrates due to ongoing sedimentation.

Hydrate reservoirs are actively maintained and the hydrate saturation profile is continuously

evolving as additional gas is transported by diffusion and dispersion down the equilibrium concentration gradient, and by advection when there is a non-zero fluid velocity. Outgassing events such as those caused by sediment failure or sea-level changes are probably responsible for moderating the hydrate content of submarine reservoirs. Continued development and refinement of hydrate accumulation models using the results of laboratory experiments and field observations will improve our understanding of this important resource.

The authors would like to thank G. R. Dickens for thoughtful comments and suggestions that have undoubtedly improved the manuscript. A. W. Rempel thanks the organizers of the First Master Conference for their excellent work and hospitality.

Appendix 1. Nomenclature

c	mass fraction of gas in fluid
$\tilde{c}$	dimensionless gas concentration $\tilde{c} \equiv (c - c_0)/\Delta c$
c_h	mass fraction of gas in hydrate
$\tilde{c}_h$	dimensionless hydrate gas concentration $\tilde{c}_h = (c_h - c_0)/\Delta c$
C	specific heat capacity at constant pressure
$\bar{C}(h)$	bulk heat capacity
$D(h)$	chemical dispersion–diffusion coefficient at hydrate pore-volume fraction h
$D(0)$	chemical dispersion–diffusion coefficient with no hydrate (i.e. $h=0$)
G	geothermal gradient
h	hydrate pore-volume fraction
H	specific enthalpy
$\bar{H}$	total enthalpy
$K(h)$	bulk thermal conductivity at hydrate pore-volume fraction h
$k(h)$	effective permeability to fluid flow at hydrate pore-volume fraction h.
l	length scale
L	latent heat of formation for hydrate
Pe	Peclet number $Pe \equiv ul/\kappa(0)$
Q	heat flux
$\Re$	reaction-rate constant for kinetic law, equation (4)
S	Stefan number $S \equiv \rho_h \phi L/(\rho_f C_f \Delta T)$
T	temperature
$\tilde{T}$	dimensionless temperature $\tilde{T} \equiv (T - T_0)/\Delta T$
t	time
$\tilde{t}$	dimensionless time $\tilde{t} \equiv t\kappa(0)/l^2$
$\mathbf{u}$	fluid velocity
z	vertical coordinate
$\tilde{z}$	dimensionless vertical coordinate $\tilde{z} \equiv z/l$
α	constant in empirical two-phase equilibrium equation (3)
ε	Lewis number $\varepsilon \equiv D(0)/\kappa(0)$
ϕ	porosity
η	dynamic viscosity of pore fluid
$\kappa(h)$	bulk thermal diffusivity $\kappa(h) \equiv K(h)/(\rho_f C_f)$
$\kappa(0)$	bulk thermal diffusivity with $h = 0$
λ	similarity coordinate for interface position
ρ	density

Subscripts

s	sediment
f	fluid
h	hydrate
0	reference value
eq	equilibrium

Appendix 2. Governing equations

The conservation equations for energy and gas are applied to a fixed volume in a continuum composed of sediment, pore fluid and hydrate. The heat equation relates the change in enthalpy H to the heat flux Q into the volume by

$$\frac{\partial H}{\partial t} = Q. \tag{B1}$$

The total enthalpy $\bar{H}$ is written as

$$\bar{H} = \rho_f H_f \phi(1 - h) + \rho_h H_h \phi h + \rho_s H_s(1 - \phi), \tag{B2}$$

where H_f, H_h and H_s are the specific enthalpies of the fluid, hydrate and sediment components. The heat flux Q into the volume may be carried by advection and conduction

$$Q = -\nabla \cdot (\rho_f H_f \mathbf{u}) + \nabla \cdot (K(h)\nabla T) \tag{B3}$$

where the advective transport is through the fluid at velocity $\mathbf{u}$, and the bulk thermal conductivity is

$K(h)$. The specific heat at constant pressure is defined as

$$C = \left.\frac{\partial H}{\partial T}\right|_p$$

and the latent heat per unit mass of hydrate is

$$L = H_f - H_h$$

We treat each of the components as incompressible and substitute (B2) and (B3) into equation (B1) using the definitions for C and L and rearranging terms to get

$$[\rho_f C_f \phi(1-h) + \rho_h C_h \phi h + \rho_s C_s(1-\phi)]\frac{\partial T}{\partial t} + \rho_f C_f \mathbf{u}\cdot\nabla T + H_f\left\{\phi(\rho_h - \rho_f)\frac{\partial h}{\partial t} + \rho_f \nabla\cdot\mathbf{u}\right\} = \nabla\cdot(K(h)\nabla T) + \rho_h \phi L \frac{\partial h}{\partial t}. \quad \text{(B4)}$$

The term in braces {} is equal to zero by conservation of mass. Dividing through by $\rho_f C_f$ we have

$$\bar{C}(h)\frac{\partial T}{\partial t} + \mathbf{u}\cdot\nabla T - \nabla\cdot(\kappa(h)\nabla T) + \frac{\rho_h \phi L}{\rho_f C_f}\frac{\partial h}{\partial t} \quad \text{(B5)}$$

where the bulk thermal diffusivity and the bulk heat capacity are

$$\kappa(h) \equiv \frac{K(h)}{\rho_f C_f} \text{ and}$$

$$\bar{C}(h) \equiv \frac{\rho_f C_f \phi(1-h) + \rho_h C_h \phi h + \rho_s C_s(1-\phi)}{\rho_f C_f}.$$

Changes in the total mass of gas in a fixed volume are due to the combined effects of advection, diffusion and dispersion. The mass of gas per unit volume is

$$\rho_f \phi c(1-h) + \rho_h \phi c_h h \quad \text{(B6)}$$

where the mass fraction of gas in the hydrate c_h may be treated as a constant. The advective gas flux into the volume through the fluid is

$$-\nabla\cdot(\rho_f c\mathbf{u}). \quad \text{(B7)}$$

We neglect the effects of the temperature gradient and the pressure gradient on the diffusive flux, and write the combined diffusive and dispersive flux as

$$\rho_f \phi \nabla\cdot((1-h)D(h)\nabla c). \quad \text{(B8)}$$

The change in the mass of gas (B6) is equal to the sum of the transport terms, equations (B7) and (B8), so that

$$\rho_f\phi(1-h)\frac{\partial c}{\partial t} + \rho_h\phi(c_h - c)\frac{\partial h}{\partial t} + \rho_f \mathbf{u}\cdot\nabla c + c\left\{\rho_f\nabla\cdot\mathbf{u} + \phi(\rho_h - \rho_f)\frac{\partial h}{\partial t}\right\} - \rho_f\phi\nabla\cdot((1-h)D(h)\nabla c). \quad \text{(B9)}$$

Dividing through by $\rho_f\phi$ and using conservation of mass to eliminate the term in braces {} we arrive at

$$(1-h)\frac{\partial c}{\partial t} + \frac{1}{\phi}\mathbf{u}\cdot\nabla c = \nabla\cdot[(1-h)D(h)\nabla c] - \frac{\rho_h}{\rho_f}(c_h - c)\frac{\partial h}{\partial t}. \quad \text{(B10)}$$

References

BANGS, N., SAWYER, D. & GOLOVCHENKO, X. 1993. Free gas at the base of the gas hydrate zone in the vicinity of the Chile triple junction. *Geology*, **21**, 905–908.

BROOKS, J., JEFFREY, A., MCDONALD, T., PFLAUM R. & KVENVOLDEN, K. 1985. Geochemistry of hydrate gas from Site 570, Deep Sea Drilling Project Leg 84. *In*: VON HUENE, R., AUBOUIN, J. *et al.* (eds) *Initial Reports of the Deep Sea Drilling Project*, Volume 84. US Government Printing Office, Washington, DC, 699–703.

BROWN, K., BANGS, N., FROELICH, P. & KVENVOLDEN, K. 1996. The nature, distribution, and origin of gas hydrate in the Chile Triple Junction region. *Earth and Planetary Science Letters*, **139**, 471–483.

CLAYPOOL, G. & KAPLAN, I. 1974. The origin and distribution of methane in marine sediments. *In*: KAPLAN, I.R. (ed.) *Natural Gases in Marine Sediments*. Plenum, New York, 99–139.

CLENNELL, M. B., HOVLAND, M., LYSNE, D. & BOOTH, J. S. 1995. Role of capillary forces, coupled flows and sediment-water depletion in the habitat of gas hydrate. *EOS Transactions of the American Geophysical Union*, **76**, S164–165.

DAVIS, E., HYNDMAN, R. & VILLINGER, H. 1990. Rates of fluid expulsion across the Northern Cascadia accretionary prism: Constraints from new heat flow and multichannel seismic reflection data. *Journal of Geophysical Research*, **95**, 8869–8889.

DICKENS, G. & QUINBY-HUNT, M. 1997. Methane hydrate stability in pore water: A simple theoretical approach for geophysical applications. *Journal of Geophysical Research*, **102**, 773–783.

——, PAULL, C., WALLACE, P. & THE ODP LEG 164 SCIENTIFIC PARTY. 1997. Direct measurement of in situ methane quantities in a large gas-hydrate reservoir. *Nature*, **385**, 426–428.

ENGLEZOS, P. & BISHNOI, P. 1988. Prediction of gas hydrate formation conditions in aqueous electrolyte solutions. *American Institute of Chemical Engineering Journal*, **34**, 1718–1721.

——, KALOGERAKIS, N., DHOLABHAI, P. & BISHNOI, P. 1987. Kinetics of formation of methane and ethane gas hydrates. *Chemical Engineering Science*, **42**, 2647–2658.

FOGG, P. & GERRARD, W. 1991. *Solubility of Gases in Liquids*. Wiley, Chichester, 113–159.

HANDA, Y. 1990 Effect of hydrostatic pressure and salinity on the stability of gas hydrates. *Journal of Physical Chemistry*, **94**, 2652–2657.

HOLBROOK, W., HOSKINS, H., WOOD, W., STEPHEN, R., LIZARRALDE, D. & THE ODP LEG 164 SCIENCE PARTY. 1996. Methane hydrate and free gas on the Blake Ridge from vertical seismic profiling. *Science*, **273**, 1840–1843.

HUPPERT, H. & WORSTER, M. 1985. Dynamic solidification of a binary melt. *Nature*, **314**, 703–707.

HYNDMAN, R. & DAVIS, E. 1992. A mechanism for the formation of methane hydrate and seafloor bottom-simulating reflectors by vertical fluid expulsion. *Journal of Geophysical Research*, **97**, 7025–7041.

—— & SPENCE, G. 1992. A seismic study of methane hydrate marine bottom simulating reflectors. *Journal of Geophysical Research*, **97**, 6683–6698.

——, WANG, K., YUAN, T. & SPENCE, G. 1993. Tectonic sediment thickening, fluid expulsion, and the thermal regime of subduction zone accretionary prisms: The Cascadia margin off Vancouver Island. *Journal of Geophysical Research*, **98**, 21, 865–21, 876.

KASTNER, M., KVENVOLDEN, K., WHITICAR, M., CAMERLENGHI, A. & LORENSON, T. 1995. Relation between pore fluid chemistry and gas hydrates associated with bottom-simulating reflectors at the Cascadia Margin, sites 889 and 992. *Proceedings of the Ocean Drilling Program, Scientific Results*, College Station, TX. Ocean Drilling Program, **146**, 175–187.

KROOS, B. & LEYTHAEUSER, D. 1988. Experimental measurements of the diffusion parameters of light hydrocarbons in water-saturated sedimentary rocks – II. Results and geochemical significance. *Organic Geochemistry*, **12**, 91–108.

KVENVOLDEN, K. 1993. Gas hydrates – Geological perspective and global change. *Reviews of Geophysics*, **31**, 173–187.

—— & BARNARD, L. 1983. Gas hydrates of the Blake Outer Ridge, Deep Sea Drilling Project Site 533, Leg 76. *In*: SHERIDAN, R., GRADSTEIN, F. *et al.* (eds) *Initial Reports of the Deep Sea Drilling Project*, Volume 75. US Government Printing Office, Washington, DC, 353–366.

LIDE, D. 1990. *CRC Handbook of Chemistry and Physics*, 71st edition. CRC, Boca Raton, FL 6–8.

MACKAY, M., JARRARD, R., WESTBROOK, G., HYNDMAN, R. & THE ODP LEG 146 SCIENCE PARTY. 1994. Origin of bottom-simulating reflectors: Geophysical evidence for the Cascadia accretionary prism. *Geology*, **22**, 459–462.

MINSHULL, T., SINGH, S. & WESTBROOK, G. 1994. Seismic velocity structure of a gas hydrate reflector, offshore western Columbia, from full waveform inversion. *Journal of Geophysical Research*, **99**, 4715–4734.

REMPEL, A. 1994. *Theoretical and Experimental Investigations into the Formation and Accumulation of Gas Hydrates*. M.Sc. thesis, University of British Columbia, Vancouver, Canada.

—— & BUFFETT, B. 1997. Formation and accumulation of gas hydrate in porous media. *Journal of Geophysical Research*, **102**, 10, 151–10, 164.

SELIM, M. & SLOAN, E. 1989. Heat and mass transfer during the dissociation of hydrates in porous media. *American Institute of Chemical Engineering Journal*, **35**, 1049–1052.

SINGH, S. & MINSHULL, T. 1994. Velocity structure of a gas hydrate reflector at ocean drilling program site 889 from a global seismic waveform inversion. *Journal of Geophysical Research*, **99**, 24, 221–24, 233.

SLOAN, E.D. 1990. *Clathrate Hydrates of Natural Gases*. Marcel Dekker, New York.

TURCOTTE, D. & SCHUBERT, G. 1982. *Geodynamics – Applications of Continuum Physics to Geological Problems*. Wiley, New York, 168–170.

TSYPKIN, G. 1991. Dissociation of gaseous hydrates in beds. *Journal of Engineering Physics*, **60**, 556–561.

—— 1992*a*. Appearance of two moving phase transition boundaries in the dissociation of gaseous hydrates in strata. *Soviet Physics Doklady*, **37**, 126–128.

—— 1992*b*. Effect of liquid phase mobility on gas hydrate dissociation in reservoirs. *Fluid Dynamics*, **26**, 564–572.

UCHIDA, T. & NARITA, H. 1996. Studies of formation and dissociation rates of methane hydrates in pure water – pure gas system. *In: Canada–Japan Joint Science and Technology Workshop on Gas Hydrates*, Victoria, Canada, 109–110.

WORSTER, M. 1992. The dynamics of mushy layers. *In*: DAVIS, S., HUPPERT, H. & MULLER, U. (eds) *Interactive Dynamics of Convection and Solidification*. Kluwer, Dordrecht, 113–138.

YAMANE, K. & AYA, I. 1995. Solubility of carbon dioxide in hydrate region at 30 MPa. *In: Proceedings of the MARIENV'95 Conference*, 911–917.

YUAN, T., HYNDMAN, R., SPENCE, G. & DESMONS, B. 1996. Seismic velocity increase and deep-sea gas hydrate concentration above a bottom-simulating reflector on the northern Cascadia continental slope. *Journal of Geophysical Research*, **101**, 13, 655–13, 671.

ZATSEPINA, O. & BUFFETT, B. 1997. Phase equilibrium of gas hydrate: Implications for the formation of hydrate in the deep seafloor. *Geophysical Research Letters*, **24**, 1567–1570.